J|A|C|S ARTICLES

Published on Web 04/09/2009

Stability and Photoelectronic Properties of Layered Titanate Nanostructures

Alexander Riss,[†] Michael J. Elser,[†] Johannes Bernardi,[‡] and Oliver Diwald*[,†,§]

Institute of Materials Chemistry, Vienna University of Technology, Veterinärplatz 1/GA, A-1210 Vienna, Austria, University Service Centre for Transmission Electron Microscopy, Vienna University of Technology, Wiedner Hauptstrasse 8-10/052, A-1040 Vienna, Austria, and Institute of Particle Technology, Friedrich-Alexander-University Erlangen-Nuremberg, Cauerstrasse 4, 91058 Erlangen, Germany

Received December 29, 2008; E-mail: odiwald@mail.zserv.tuwien.ac.at

Abstract: Layered titanate nanostructures offer promising photoelectronic properties that are subject to surface chemistry-induced morphology changes. For a systematic evaluation of the bulk and surface contributions to the photoactivity of these structures, we investigated their photoelectronic properties and in particular their dependence on the condition of the gas−solid interface. We comprehensively explored the stability of $Na_2Ti_3O_7$ nanowires and scrolled up $H_2Ti_3O_7$ nanotubes by means of transmission electron microscopy, Raman, and FT-IR spectroscopy and subjected both titanate sheet-based structures to controlled thermal activation treatment under high vacuum conditions. We found that throughout thermal annealing up to $T = 870$ K the structure and morphology of $Na_2Ti_3O_7$ nanowires are retained. Consistent with the significant photoluminescence emission that is attributed to radiative exciton annihilation in the bulk, UV-induced charge separation is strongly suppressed in these structures. $H_2Ti_3O_7$ nanotubes, however, undergo transformation into elongated anatase nanocrystals during annealing at temperatures $T \geq 670$ K. Photoexcitation experiments in O_2 atmosphere reveal that these structures efficiently sustain the separation of photogenerated charges. Trends in the abundance of trapped holes and scavenged electrons were characterized quantitatively by tracking the concentration of paramagnetic O^- and O_2^- species with electron paramagnetic resonance spectroscopy EPR, respectively. An incisive analysis of these results in comparison to those obtained on airborne anatase nanocrystals underlines the critical role of surface composition and structure on charge separation and, in consequence, on the chemical utilization of photogenerated charge carriers.

Introduction

Advances in materials synthesis have made a large number of particulate nanostructures available that display improved uniformity in terms of size, structure, and morphology. Access to such materials is essential for uncovering their intrinsic and usable properties, which are less affected by sample heterogeneity.[1−3] Beyond synthesis, the controlled integration of these structures into larger functional devices represents a next challenge toward their efficient utilization. For this purpose, nanoparticles need to be processed, assembled, and immobilized, and related procedures typically involve thermal activation steps.

Substantial efforts have been devoted to the synthesis of TiO_2- and TiO_2-based materials mainly due to their great technological potential for photovoltaic and photocatalytic applications.[4−6] Many of these, spanning wastewater treatments, self-cleaning surfaces, to water splitting photoelectrodes, share the fact that the overall performance results from a combination of effects that start with photoexcitation of the bulk and end with interfacial charge transfer and chemical activation of molecules at the particle surface. The large number of conflicting reports concerning the activity of TiO_2 based materials arises from the fact that these materials were obtained by different synthesis techniques, subjected to varying preactivation steps, and last but not least characterized in very different chemical environments. A very recent study by Ryu and Choi[7] revealed that the "photocatalytic activity" of a particular TiO_2 powder material largely depends on the choice of the test reaction and that there is no single and general figure of merit with respect to this function. Thus, advances in the development of more efficient materials rely on comprehensive characterization work that addresses the fundamental processes contributing to the overall photochemical reaction and focuses on their mutual interplay to identify rate- and performance-determining factors. These, in turn, critically depend on the fundamental particle bulk properties composition, structure, and morphology, on the one hand, and area and quality of the surface, on the other.[8−12]

[†] Institute of Materials Chemistry.
[‡] University Service Centre for Transmission Electron Microscopy.
[§] Friedrich-Alexander-University Erlangen-Nuremberg.

(1) Yin, Y.; Alivisatos, A. P. *Nature (London)* **2005**, *437*, 664–670.
(2) Burda, C.; Chen, X. B.; Narayanan, R.; El-Sayed, M. A. *Chem. Rev.* **2005**, *105*, 1025–1102.
(3) Pileni, M. P. *J. Phys. Chem. C* **2007**, *111*, 9019–9038.
(4) Thompson, T. L.; Yates, J. T. *Chem. Rev.* **2006**, *106*, 4428–4453.
(5) Hoffmann, M. R.; Martin, S. T.; Choi, W.; Bahnemann, D. W. *Chem. Rev.* **1995**, *95*, 69–96.
(6) Kongkanand, A.; Tvrdy, K.; Takechi, K.; Kuno, M.; Kamat, P. V. *J. Am. Chem. Soc.* **2008**, *130*, 4007–4015.
(7) Ryo, J.; Choi, W. *Environ. Sci. Technol.* **2008**, *42*, 294–300.

10.1021/ja810109g CCC: $40.75

In the course of nanomaterials' synthesis and characterization, layered titanate nanostructures have attracted much attention partly because of a huge variety of potential applications[13−16] but also because of their intriguing structure and morphology changes induced by surface chemistry.[17] The materials have become available in various morphological forms, with scrolled up titanate nanotubes as the most prominent ones.[13,14,18] Hydrothermal treatment of TiO_2 powders in strong alkaline aqueous solutions[19] or their refluxing under atmospheric pressures[20] have been employed as a very simple production method. Using hydrothermal synthesis, subtle changes in the synthesis conditions were found to lead to marked differences in the structural properties, and a more comprehensive examination of the relationship between hydrothermal parameters, product morphology, and phase has been reported only recently.[21−24] Anatase-TiO_2, lepidocrocite, and protonated titanates of the $H_2Ti_3O_7$ type are closely related from a structural point of view and have been proposed as possible constituents of nanotubes.[25−27] In fact, spontaneous rearrangement from one form into the other can easily occur and is expected to be driven by changes in the local water partial pressure.[28] In a foregoing study, we reported on surface chemistry-induced morphology transformation of layered titanate nanostructures and its effect on the photoelectronic properties. There is a clear complementarity between titanate morphologies that are associated with photoluminescence in conjunction with inhibited separation of photogenerated charges and those with the opposite properties.[29] Respective trends as well as the branching ratio between radiative deactivation of photoexcited states,[30] on the one hand, and their chemical utilization, on the other, can easily be controlled by solution chemistry. Because of the variety of related applications that are based on gas solid interface effects,[31,32] there is growing need of surface science investigations on these structures. However, to the best of our knowledge, there is hardly any investigation that addresses the solid gas interface to date. This may be reasoned in a number of complications, which arise from the fact that nanomaterials basically are surface determined solids requiring additional materials' characterization work. Addition or removal of solvent molecules to or from the surface may cause substantial changes in structure and morphology.[33] Considering this, we subjected titanate nanosheets either protonated and arranged as scrolled up $H_2Ti_3O_7$ nanotubes,[34,35] or as flat $Na_2Ti_3O_7$ nanowires where the stacked sheets contain sodium ions in the interlayer region, to thermal activation procedures in controlled gas atmospheres. Aiming at the identification of material-specific factors that determine the fate of photoexcited states, we carefully tracked phase and morphology as a function of annealing temperature. Knowing these fundamental materials' properties, we employed FT-IR, photoluminescence, and electron paramagnetic resonance (EPR) spectroscopy to investigate the surface coverage with adsorbates, on the one hand, and the photoelectronic properties associated with the particular nanostructure, on the other. Special attention has been paid to the quality of the surface, which critically affects the trapping process of photogenerated charges.

Experimental Section

In a typical synthesis procedure, 5 g of commercial anatase powder (Alfa Aesar no. 36199) was treated with 300 mL of 10 N NaOH at $T = 380$ K under reflux conditions for 48 h. The obtained product will be referred to as $Na_2Ti_3O_7$ titanate nanowires. A part of the sample was treated with 0.1 N HCl four times to yield proton exchanged titanate nanotubes ($H_2Ti_3O_7$). Both samples were washed with distilled water followed by drying at room temperature.

Transmission electron microscopy images were obtained using a TECNAI F20 analytical microscope equipped with a S-Twin objective lens and a field emission source operating at 200 kV. Images were recorded with a Gatan 794 Multiscan CCD camera.

For EPR measurements, approximately 20 mg of the powder sample is contained within a Suprasil quartz glass tube, which is connected to an appropriate high vacuum pumping system providing base pressures better than $p = 10^{-6}$ mbar. A 300 W Xe lamp (Oriel) was employed as the UV source. The light beam was passed through a water filter to exclude IR contributions from the excitation spectrum. Light power was measured with a bolometer (International Light) and kept constant at 0.7 mW cm^{-2} (10^{15} photons s^{-1} cm^2) for the wavelength range 200 nm $\leq \lambda \leq$ 380 nm throughout all experiments. X-band EPR measurements were performed with a Bruker EMX 10/12 spectrometer using an ER 4102 ST standard rectangular resonant cavity in the TE102 mode. Low-temperature measurements were carried out with an ER 4131 VT variable temperature accessory, which operates in the temperature range between 90 and 300 K. The g values were determined on the basis of a diphenylpyricylhydrazil (DPPH) standard.

A pulsed Xe discharge lamp served as the excitation light source in a Perkin-Elmer LS 50B system for low-temperature photoluminescence measurements. Measurements were carried out at 77 K using a commercially available low-temperature luminescence accessory where the sample cell was held by a high-purity copper

(8) Testino, A.; Bellobono, I. R.; Buscaglia, V.; Canevali, C.; D'Arienzo, M.; Polizzi, S.; Scotti, R.; Morazzoni, F. *J. Am. Chem. Soc.* **2007**, *129*, 3564–3575.
(9) Feldhoff, A.; Mendive, C.; Bredow, T.; Bahnemann, D. *ChemPhysChem* **2007**, *8*, 805–809.
(10) Li, G.; Gray, K. A. *Chem. Phys.* **2007**, *95*, 173–187.
(11) Gong, X. G.; Selloni, A.; Batzill, M.; Diebold, U. *Nat. Mater.* **2006**, *5*, 665–670.
(12) Wu, B.; Guo, C.; Zheng, N.; Xie, Z.; Stucky, G. D. *J. Am. Chem. Soc.* **2008**, *130*, 17563–17567.
(13) Mao, Y.; Park, T. J.; Zhang, F.; Zhou, H.; Wong, S. S. *Small* **2007**, *3*, 1122–1139.
(14) Bavykin, D.; Friedrich, J.; Walsh, F. *Adv. Mater.* **2006**, *18*, 2807–2824.
(15) Macak, J. M.; Tsuchiya, H.; Ghicov, A.; Yasuda, K.; Hahn, R.; Bauer, S.; Schmuki, P. *Curr. Opin. Solid State Mater. Sci.* **2007**, *11*, 3–18.
(16) Grimes, C. A. *J. Mater. Chem.* **2007**, *17*, 1451–1457.
(17) Zhu, H. Y.; Lan, Y.; Gao, X. P.; Ringer, S. P.; Zheng, Z. F.; Song, D. Y.; Zhao, J. C. *J. Am. Chem. Soc.* **2005**, *127*, 6730–6736.
(18) Chen, Q.; Peng, L. M. *Int. J. Nanotechnol.* **2007**, *4*, 44–65.
(19) Kasuga, T.; Hiramatsu, M.; Hoson, A.; Sekino, T.; Niíhara, K. *Langmuir* **1998**, *14*, 3160–3163.
(20) Bavykin, D. V.; Cressey, B. A.; Light, M. E.; Walsh, F. C. *Nanotechnology* **2008**, *19*, 275604.
(21) Morgan, D. L.; Zhu, H. Y.; Frost, R. L.; Waclawik, E. R. *Chem. Mater.* **2008**, *20*, 3800–3802.
(22) Mao, Y. B.; Wong, S. S. *J. Am. Chem. Soc.* **2006**, *128*, 8217–8226.
(23) Nian, J. N.; Teng, H. *J. Phys. Chem. B* **2006**, *110*, 4193–4198.
(24) Tsai, C. C.; Teng, H. *Chem. Mater.* **2006**, *18*, 367–373.
(25) Vittadini, A.; Casarin, M. *Theor. Chem. Acc.* **2008**, *120*, 551–556.
(26) Vittadini, A.; Casarin, M.; Selloni, A. *Theor. Chem. Acc.* **2008**, *1178*, 663–671.
(27) Pradhan, S. K.; Mao, Y.; Wong, S. S.; Chupas, P.; Petkov, V. *Chem. Mater.* **2007**, *19*, 6180–6186.
(28) Vittadini, A.; Casarin, M.; Selloni, A.; Casarin, M.; Vittadini, A.; Selloni, A. *ACS Nano* **2009**, *3*, 317–324.
(29) Riss, A.; Berger, T.; Stankic, S.; Bernardi, J.; Knözinger, E.; Diwald, O. *Angew. Chem., Int. Ed.* **2008**, *47*, 1496–1499.
(30) Riss, A.; Berger, T.; Grothe, H.; Bernardi, J.; Diwald, O.; Knözinger, E. *Nano Lett.* **2007**, *7*, 433–438.
(31) Diebold, U. *Surf. Sci. Rep.* **2003**, *48*, 53–229.
(32) Gurlo, A.; Riedel, R. *Angew. Chem., Int. Ed.* **2007**, *46*, 3826–3848.
(33) Zhang, H.; Gilbert, B.; Huang, F.; Banfield, J. F. *Nature (London)* **2003**, *424*, 1025–1029.
(34) Teng, C. C.; Teng, H. *Chem. Mater.* **2006**, *18*, 367–373.
(35) Poudel, B.; Wang, W. Z.; Dames, C.; Huang, J. H.; Kunwar, S.; Wang, D. Z.; Banerjee, D.; Chen, G.; Ren, Z. F. *Nanotechnology* **2005**, *16*, 1935–1940.

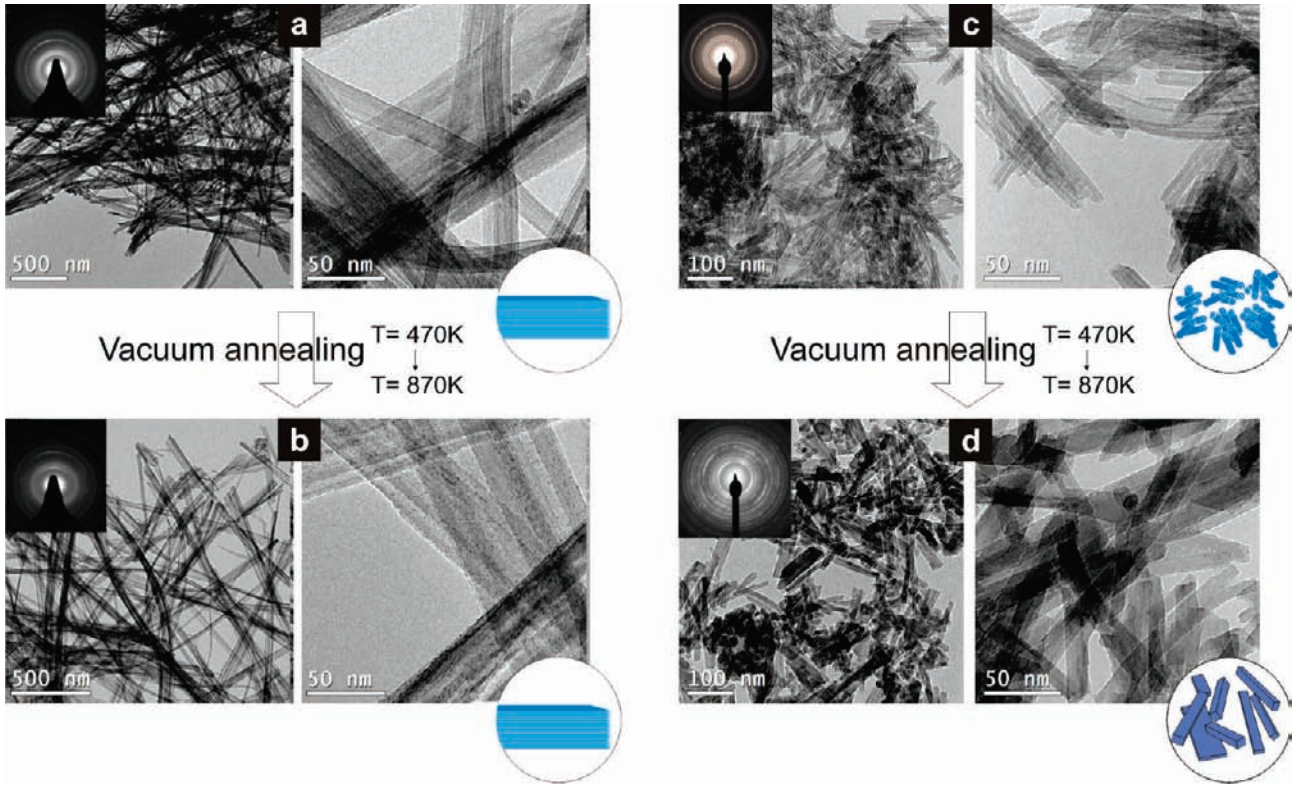

Figure 1. Transmission electron micrographs of nanowires (a,b) and nanotubes (c,d) after vacuum annealing and subsequent reoxidation at $T = 470$ K (a,c) and $T = 870$ K (b,d). Whereas $Na_2Ti_3O_7$ nanowires retain their morphology throughout annealing up to $T = 870$ K, protonated nanotubes transform into massive rod-like structures at temperatures $T \geq 670$ K. Insets show selected area electron diffraction patters, which for the nanotubes indicate a structural transformation from the trititanate phase into TiO_2 anatase.

rod that was immersed in liquid nitrogen. Room-temperature excitation and emission spectra were acquired with a Fluorolog-3 FL322 spectrofluorometer equipped with double grating monochromators (both at the excitation and at the emission side) and a photodiode reference detector. A 450 W xenon lamp was used as the excitation light source; the emitted light was detected by a R928P (Hamamatsu) photomultiplier operating in photon counting mode.

The nitrogen sorption isotherms were obtained at 77 K using an adsorption porosimeter (Micromeritics ASAP 2020). The BET surface area S_{BET} was evaluated using adsorption data in a relative pressure range p/p_0 from 0.05 to 0.2. Raman spectra were obtained with a microscope system (Horiba Jobin Yvon, LabRAM HR) using a He−Ne laser (632.8 nm) for excitation. The Raman-scattered light was collected at 180°, dispersed by an optical grid, and detected by a CCD camera with a spectral resolution of 4 cm^{-1}.

For transmission FT-IR spectroscopy, a high vacuum cell developed by J. T. Yates Jr. and co-workers[36,37] was used and for this purpose aligned in the optical path of the IR beam of a Bruker Tensor 27 spectrometer system. The resolution was 3 cm^{-1}, and 200 interferogram scans were averaged to guarantee a reasonable signal-to-noise ratio. Typically, 2 mg of powder sample was pressed into a tungsten grid, which was then subsequently mounted in the high vacuum cell that provides a base pressure $p < 10^{-7}$ mbar. This setup enables controlled sample annealing and sample measurement at well-defined pressures in the range 10^{-7} mbar $\leq p \leq 10^3$ mbar. Sample activation procedures were identical to those related to photoluminescence and EPR measurements.

Results

$Na_2Ti_3O_7$ nanowires obtained by reflux treatment of commercial TiO_2 anatase powders in aqueous NaOH solutions[38,39] show a high aspect ratio with widths of about 50−100 nm and lengths up to micrometers (Figure 1). Lattice fringes of 0.75 ± 0.05 nm reveal the presence of stacked polyanion sheets, which are made of interconnected [TiO_6] octahedra (Figure 1a). Charge neutrality within these complete structures is provided by Na^+ ions in the interlayer region.[30]

$H_2Ti_3O_7$, on the other hand, can be characterized as scrolled up hollow structures with inner diameter of 12 nm, outer diameter of 4 nm, and lengths of about 100 nm (Figures 1c and 2).[30] Consistent with their smaller size, the respective material has a specific surface area of 280 m^2/g, which is by a factor of 2 larger than that related to the wires with $S_{BET} = 130$ m^2/g. For both materials, high-resolution transmission electron micrographs reveal relatively smooth surfaces and parallel-oriented lattice fringes with interlayer spacings of 0.75 ± 0.05 nm.

The investigation of the gas−solid interface requires elimination of surface adsorbates prior to the respective experiment. Therefore, we subjected both types of nanostructures to annealing at temperatures in the range 298 K $\leq T \leq$ 870 K at pressures $p < 10^{-5}$ mbar. Transmission electron micrographs of nanowires and nanotubes treated at $T = 470$ K, $T = 670$ K, and $T = 870$ K clearly show that nanowires retain their morphology up to T

(36) Basu, P.; Ballinger, T. H.; Yates, J. T. *Rev. Sci. Instrum.* **1988**, *59*, 1321–1327.
(37) Panayotov, D. A.; Yates, J.-T. *Chem. Phys. Lett.* **2005**, *410*, 11–17.
(38) Kasuga, T.; Hiramatsu, M.; Hoson, A.; Sekino, T.; Niihara, K. *Adv. Mater.* **1999**, *11*, 1307–1311.
(39) Yang, J.; Jin, Z.; Wang, X.; Li, W.; Zhang, J.; Zhang, S.; Guo, X.; Zhang, Z. *Dalton Trans.* **2003**, 3898–3901.

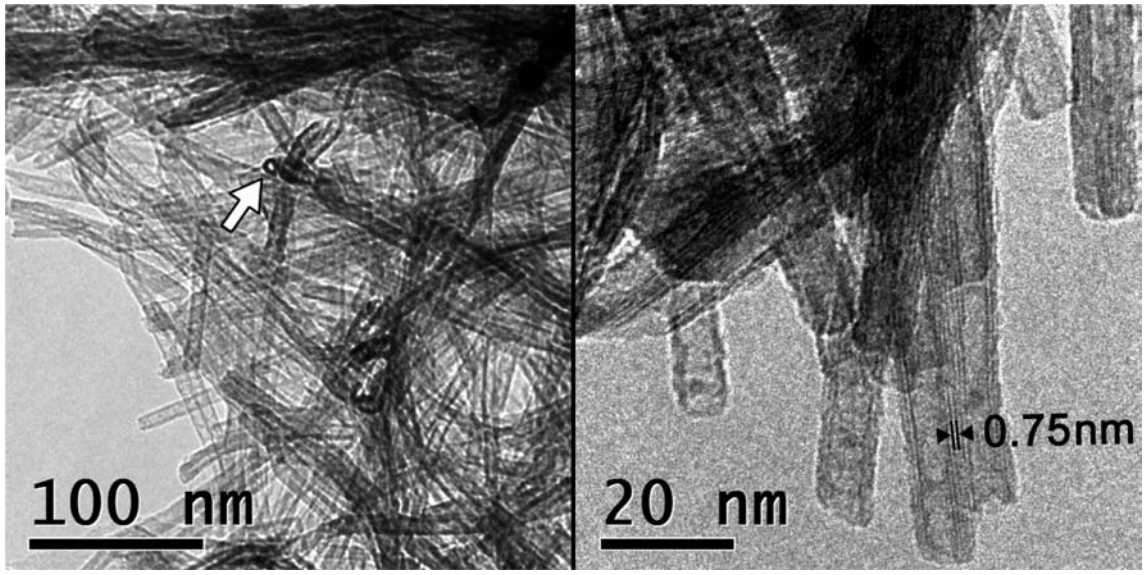

Figure 2. High-resolution transmission micrographs of $H_2Ti_3O_7$ nanostructures of uniform tubular morphology and dimensions. The white arrow in the left-hand image points to a nanotube, which is imaged in sectional top view and indicates its hollow structure.

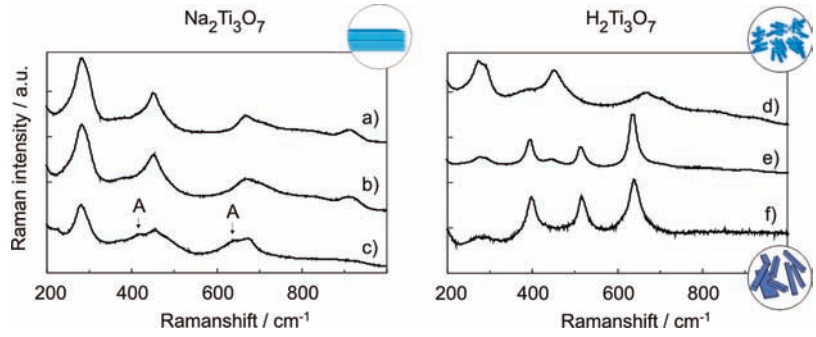

Figure 3. Raman spectra of $Na_2Ti_3O_7$ nanowires (a−c) and $H_2Ti_3O_7$ nanotubes (d,e) after annealing to $T = 470$ K, $T = 670$ K, and $T = 870$ K, respectively. Whereas the nanowires retain their crystallographic structure over the entire temperature range, nanotubes transform into TiO_2 anatase at sample activation temperatures above $T = 670$ K.

$= 870$ K, while, starting at $T = 670$ K, nanotubes are subject to significant annealing-induced morphology changes. The respective transformation is characterized by the collapse of hollow structures upon formation of complete rod-like particles with relatively flat surfaces (Figure 1d). We carried out electron diffraction (Figure 1) as well as Raman spectroscopy measurements (Figure 3) to track annealing-induced changes in structure. For powder activation at $T = 470$ K, both $Na_2Ti_3O_7$ nanowires and $H_2Ti_3O_7$ nanotubes show Raman features that are consistent with those of the trititanate structure.[30,40] In the case of $Na_2Ti_3O_7$ nanowires, the Raman spectra related to samples that were gradually annealed at temperatures up to $T = 870$ K (Figure 3b and c) exhibit essentially no changes as compared to the situation before annealing (Figure 3a). Only features of minor intensity (see As in Figure 3c) can be observed for a powder that was previously treated at $T = 870$ K and point to the starting phase transformation into TiO_2 anatase. The respective situation is very different for $H_2Ti_3O_7$ nanotubes: structure and morphology of these particles survive prolonged annealing ($t \leq 5$ h) at temperatures below or equal to $T = 470$ K. However, thermal activation at $T \geq 670$ K induces phase transformation. In line with the TEM data (Figure 1d), electron diffraction and Raman spectroscopy indicate that the particle structure transforms from the trititanate modification (Figures 1c and 3d) into the anatase modification of TiO_2 (Figures 1d and 3f). These fundamental changes in the particle properties are also reflected by the macroscopic changes: after annealing at $T = 670$ K, the powder volume of the nanotubes sample decreases to about one-third of its original value.

In reducible oxides such as TiO_2, vacuum treatment at elevated temperatures is associated with lattice oxygen removal and thermally induced substoichiometry.[31] In the course of oxygen depletion, the valence state of negatively charged O^{2-} lattice anions changes from -2 to zero upon formation of neutral O species that then become removed from the solid. Associated electrons remain either distributed over the particle in form of conduction band electrons[41] or localized at titanium ions in form of paramagnetic Ti^{3+}.[42] The latter type of defect is accessible to EPR spectroscopy (see Figure S3, Supporting Information), and related concentrations were quantified for $H_2Ti_3O_{7-x}$ and $Na_2Ti_3O_{7-x}$ powder samples. After annealing to $T = 670$ K, the spin concentrations amount to 400 and 7 μmol g^{-1} for

(40) Ma, R.; Fukuda, K.; Sasaki, T.; Osada, M.; Bando, Y. *J. Phys. Chem. B* **2005**, *109*, 6210–6214.

(41) Berger, T.; Sterrer, M.; Diwald, O.; Knözinger, E.; Panayotov, D.; Thompson, T. L.; Yates, J. T. *J. Phys. Chem. B* **2005**, *109*, 6061–6068.

(42) Berger, T.; Diwald, O.; Knözinger, E.; Napoli, F.; Chiesa, M.; Giamello, E. *Chem. Phys.* **2007**, *339*, 138–145.

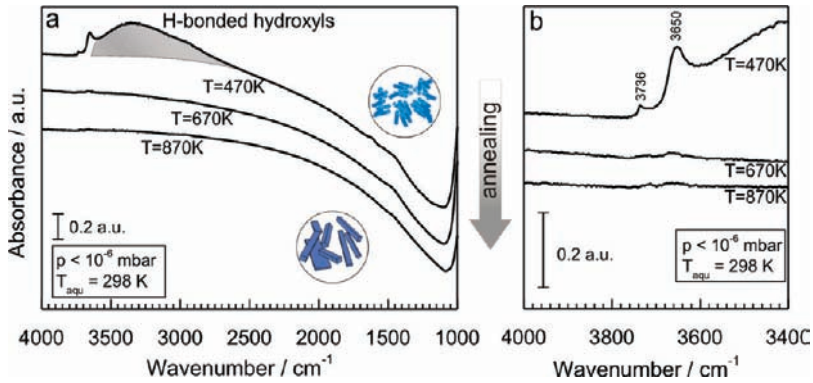

Figure 4. Transmission FT-IR spectra of $H_2Ti_3O_7$ nanotubes after vacuum annealing at $T = 470$ K (a), 670 K (b), and 870 K (c).

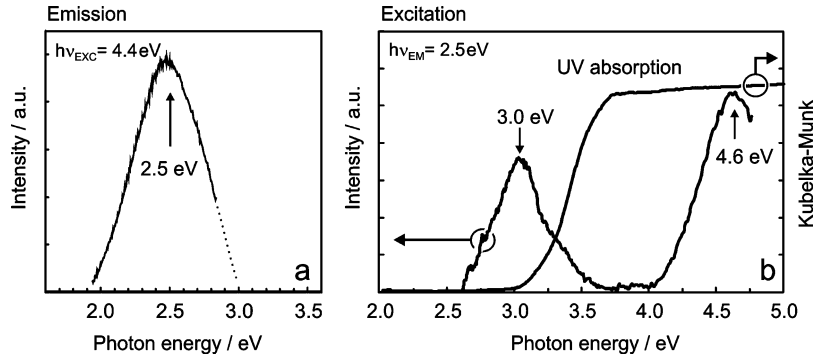

Figure 5. (a) Room-temperature photoluminescence emission spectrum of $Na_2Ti_3O_7$ nanowires[45] using excitation light of $h\nu_{EXC} = 4.4$ eV. Figure 5b shows the corresponding excitation spectrum (PL) in comparison with the optical absorption curve (UV diffuse reflectance spectroscopy).[30]

$H_2Ti_3O_{7-x}$ and $Na_2Ti_3O_{7-x}$, respectively. Thus, lattice oxygen depletion is significantly facilitated in highly dispersed $H_2Ti_3O_7$ nanotubes, which also undergo structural transformation. Another aspect related to lattice oxygen removal is that optical absorptions in the range of visible light usually arise from the concomitant electronic reduction of the solid (Figure S4, Supporting Information). For the investigation of light-induced processes, resulting optical self-absorption effects need to be eliminated. Therefore, we subjected every sample type to oxygen treatment at the respective temperature chosen during vacuum annealing carried out before. Such a procedure effectively bleaches out the color of the oxygen-deficient nanoparticle powder, annihilates Ti^{3+} sites, and on this basis is believed to restore stoichiometry.

Despite the significant difference in the concentration of constitutional hydroxyls between $Na_2Ti_3O_7$ titanate nanowires and $H_2Ti_3O_7$ nanotubes, we measured very similar absorption spectra for the two types of samples (Figures 4 and S5, Supporting Informations). For this reason, only the spectra related to $H_2Ti_3O_7$ nanotubes (Figure 4) will be discussed. The top trace in Figure 4a corresponds to a survey spectrum acquired from $H_2Ti_3O_7$ nanotubes after annealing to $T = 470$ K. It clearly reveals the broad and unspecific absorption between 3600 and 2500 cm^{-1}. This feature was also observed on $Na_2Ti_3O_7$ nanowire samples and is indicative of the presence of H-bonded hydroxyls. In addition, two distinct bands were observed at 3736 and 3650 cm^{-1}, which are attributed to free and isolated hydroxyls containing single and multiple coordinated oxygen ions, respectively.[43] After vacuum annealing and subsequent reoxidation at $T = 670$ K, the entire spectral range between 4000 and 1000 cm^{-1} is exempt of any significant IR absorption band. Because the same is true for $Na_2Ti_3O_7$ nanowires (see Figure S5, Supporting Informations), we conclude that there is no characteristic IR contribution of constitutional hydroxyls, which are only specific to the $H_2Ti_3O_7$ nanotubes. This either may be due to their low relative abundance in comparison of those at the outer surfaces of the respective nanostructures or may be attributed to the low IR-activity of this type of hydroxyl groups. Finally, we want to note that under the same experimental conditions applied, we found that hydrogen-bonded neighboring hydroxyls at the surface of airborne TiO_2 nanocrystals[41] exhibit a significantly decreased thermal stability and can be entirely eliminated by vacuum annealing at $T = 470$ K.[44]

For the two types of layered titanate nanostructures, we found a clear complementarity between the radiative deactivation of photoexcited states and the concentration of paramagnetic reaction products that originate from persistent charge separation.[29] $Na_2Ti_3O_7$ nanowires as well as scrolled-up $H_2Ti_3O_7$ nanotubes display optical band gaps at identical positions, at $E_{bg} = 3.2$ eV.[30] Substantial photoluminescence emission, however, was only observed for $Na_2Ti_3O_7$ nanowires: excitation at $h\nu_{EXC} = 4.4$ eV ($\lambda_{EXC} = 282$ nm) produces a photoemission band centered around 2.5 ± 0.1 eV (500 nm)[45] (Figure 5).

The associated excitation spectrum displays two maxima, one at 3.0 eV, which is 0.2 eV below the measured absorption threshold (UV diffuse reflectance), and a second one at 4.6 eV

(43) (a) Takeuchi, M.; Martra, G.; Coluccia, S.; Anpo, M. *J. Phys. Chem. C* **2007**, *111*, 9811–9817. (b) Diwald, O.; Sterrer, M.; Knözinger, E. *Phys. Chem. Chem. Phys.* **2002**, *4*, 2811–2817. (c) Knözinger, E.; Jacob, K. H.; Singh, S.; Hofmann, P. *Surf. Sci.* **1993**, *290*, 388–402.

(44) Elser, M. J.; Berger, T.; Brandhuber, D.; Bernardi, J.; Diwald, O.; Knözinger, E. *J. Phys. Chem. B* **2006**, *110*, 7605–7608.

(45) With regard to previous studies carried out in our laboratory, we used for the present experiment a spectrometer system with a stronger light source in conjunction with a significantly improved scattered light suppression. On this basis, we were able to monitor substantial PL emission from $Na_2Ti_3O_7$ nanowires already at room temperature.

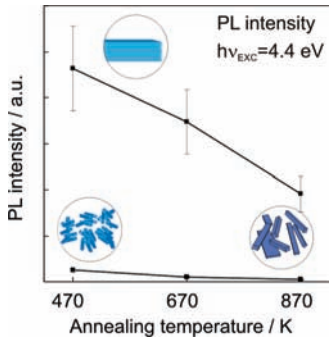

Figure 6. Photoluminescence emission intensities related to $Na_2Ti_3O_7$ nanowires (upper curve) and $H_2Ti_3O_7$ nanotubes (lower curve) as a function of temperature of annealing, which was applied prior to spectroscopy. After treatment at the indicated temperature and under high vacuum conditions ($p < 10^{-5}$ mbar), reoxidation with molecular oxygen was carried out to exclude possible self-absorption effects (see Figure S4c, Supporting Informations). The experimental data were corrected for changes in the density of the powder contained in the sample cell. Consequently, the plotted values correspond to identical quantities of sampled material. During spectrum acquisition, the samples were kept at $T = 77$ K.

(Figure 5b). A systematic evaluation of the influence of thermal activation on the photoluminescence emission properties (Figure 6) revealed for $Na_2Ti_3O_7$ nanowires that the intensity of the emission band at 2.5 ± 0.1 eV decreases considerably with increasing annealing temperature: after activation at $T = 870$ K, the respective value corresponds only to the half of that related to the material after dehydration at $T = 470$ K. In agreement with a previous study,[30] the emission properties were found to be independent of the surrounding gas atmosphere, that is, oxygen ($p = 10$ mbar) or pressures below $p < 10^{-5}$ mbar.

By means of electron paramagnetic resonance spectroscopy, we employed the photogeneration of paramagnetic species[46−48] for the quantification of persistently trapped charges.[49] In a typical experiment, the powder sample was exposed for a time of $t = 2400$ s to UV light of a constant flux of photons (10^{15} photons s^{-1} cm^2 with photon energies $h\nu \geq 3.2$ eV). A temperature of $T = 140$ K was selected to keep UV-induced heating effects constant[50] and to also prevent O_2 condensation within the sample cell at the same time. Experiments were carried out in a vacuum ($p < 10^{-5}$ mbar) as well as in the presence of molecular oxygen ($p(O_2) = 7.0$ mbar). Because of the electron scavenging activity of molecular oxygen,[41,49] the latter procedure leads to the substantial enhancement in charge separation by a factor of 2. While $Na_2Ti_3O_7$ nanowires show a negligible concentration of paramagnetic species, $H_2Ti_3O_7$ nanotubes (Figure 7a) as well as anatase nanorods derived therefrom (Figure 7c) clearly contain paramagnetic species, the EPR parameters of which are consistent with those of oxygen centered radicals (Table 1).

Depending on the temperature of annealing, we observed profound changes in the EPR signals' shape (Figure 7a−c), which indicates that more than one type of oxygen radical

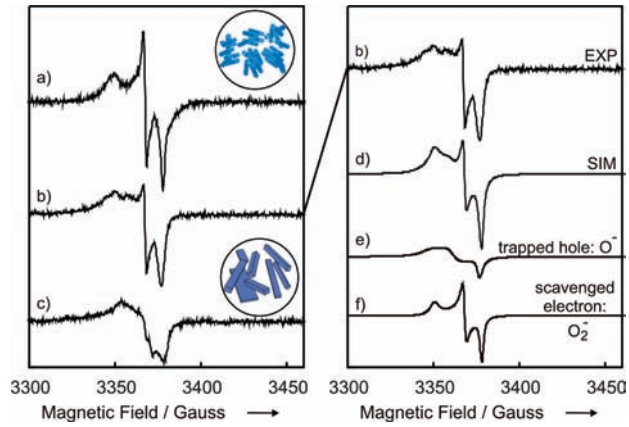

Figure 7. EPR spectra after UV irradiation of nanotubes that were previously annealed at $T = 470$ K (a), $T = 670$ K (b), and $T = 870$ K (c). The spectra related to nanotubes activated at $T = 670$ K (b) can be simulated by the addition of spectra for paramagnetic hole centers (O^-) and scavenged electrons in the form of superoxide anions (O_2^-).

Table 1. *g* Parameters of Paramagnetic Oxygen Species (Figure 6e and f) Detected on $H_2Ti_3O_7$ Nanotubes

	g parameters		
	g_{zz}	g_{yy}	g_{xx}
trapped hole: O^-	2.0210	2.0135	2.0042
scavenged electron: O_2^-	2.0198	2.0093	2.0033

contributes to the overall feature. In fact, we found that the entire set of experimental spectra can be decomposed into the components of essentially two species,[51] trapped holes (O^-) as well as adsorbed O_2^- species that correspond to scavenged electrons. As an example, the spectrum related to $H_2Ti_3O_7$ nanotubes that were previously annealed to $T = 670$ K (Figure 7b) shows a reasonably good agreement with the result of spectrum simulation: on the basis of the parameters in Table 1, the simulated single spectra e and f add up to the curve in Figure 7d, which is consistent with the respective experimental spectrum in Figure 7b. While paramagnetic trapped hole centers are essentially absent on material previously subjected to annealing at $T = 470$ K (note the good agreement between the experimental curve in Figure 7a with the simulated powder spectrum of O_2^- anions in Figure 7f), there is roughly a 1:1 ratio between trapped holes (O^-) and scavenged electrons (O_2^-) on $H_2Ti_3O_7$ nanotubes that were previously annealed to $T = 670$ K. Furthermore, we learned that the O^- radicals do correspond to shallowly trapped hole centers because raising the temperature from $T = 140$ K to $T = 298$ K leads to annihilation of related signals, which is different from O_2^- ions, the related signal intensity of which remains unaffected after such a step. Spectrum simulations were also carried out for the experimental spectra in Figure 7a and c (see Supporting Information). On the basis of a previously developed procedure for the quantification of radicals that originate from photoinduced charge separation, we determined the yield of paramagnetic species related to the various nanostructures obtained by different annealing treatment prior to the spectroscopic experi-

(46) Che, M.; Tench, A. J. *Adv. Catal.* **1983**, *32*, 1–148.
(47) Anpo, M.; Che, M.; Fubini, B.; Garrone, E.; Giamello, E.; Paganini, M. C. *Top. Catal.* **1999**, *8*, 189.
(48) Carter, E.; Carley, A. F.; Murphy, D. M. *J. Phys. Chem. C* **2007**, *111*, 10630–10638.
(49) Berger, T.; Sterrer, M.; Diwald, O.; Knözinger, E. *ChemPhysChem* **2005**, *6*, 2104–2112.
(50) Berger, T.; Diwald, O.; Knözinger, E.; Sterrer, M.; Yates, J. T. *Phys. Chem. Chem. Phys.* **2006**, *8*, 1822–1826.

(51) As reported elsewhere, a paramagnetic defect at $g = 2.0031$ is additionally observed on samples that were preannealed at $T = 470$ K. The EPR properties of this center are consistent with those of electron centers identified in aggregated TiO_2 nanocrystals. We expect that the associated defect is located underneath the surface because only limited interaction with paramagnetic O_2 from the gas phase was observed.

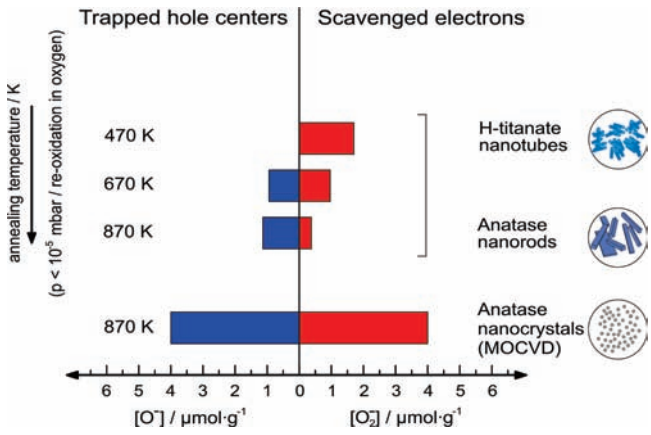

Figure 8. Quantification of paramagnetic species isolated after UV-induced charge separation on titanate nanotubes, anatase nanorods, and essentially spherical anatase nanocrystals. The latter powder material consists of anatase nanoparticles with an extremely narrow size distribution, which were obtained by metal organic chemical vapor deposition as a solvent-free synthesis technique.[41]

ment (Figure 8). The total number of paramagnetic species remains constant within the experimental uncertainty ± 30%. However, the ratio of the scavenged electrons to trapped holes varies: whereas the relative abundance of O_2^- radicals decreases with annealing temperature, the relative abundance of O^- actually increases. For comparison with previous work, we also included data from airborne anatase nanocrystals of highly irregular shape and thus with particularly complex surface structures.[49] After UV exposure under conditions identical to those applied to the titanate nanostructures, the measured concentration of separated charges is by a factor of 4 higher.

Discussion

Structure and Morphology. Advances in the synthesis of unsupported functional nanostructures[2,8,12,52−54] have prompted the investigation of size- and morphology-related physical and chemical properties of solids. In this regard, it has been shown that an ensemble of morphologically well-defined particles can exhibit specific functional interface features, the concentration of which is negligibly small in macroscopic systems.[55−57] Structurally, $Na_2Ti_3O_7$ nanowires and $H_2Ti_3O_7$ nanotubes are composed of two-dimensional titanate nanosheets,[25−27,58] which either form scrolled up and open ended nanotubes or exist as flat structures such as $Na_2Ti_3O_7$ nanoribbons and wires.[14,19,30] Because of their high dispersion, the structure and morphology of these materials are subject to the condition of the surface. Consequently, annealing-induced dehydration and dehydroxylation (Figure 4) plays a critical role. Vittadini et al.[28] predicted on the basis of periodic density functional calculations that water adsorption converts lepidocrocite nanosheets either into stepped protonated titanates[27] or into hydroxylated nanosheets of delaminated anatase.[59,60] Apart from the fact that hydration and hydroxylation determines the intrinsic stability of the nanosheet, it also affects interlayer interactions and, thus, the curvature of the titanate layers.[61] In the course of the present study, we learned that $Na_2Ti_3O_7$ nanowires retain their structure and morphology over the entire temperature range explored, that is, 470 K ≤ T ≤ 870 K. $H_2Ti_3O_7$ nanotubes, however, are susceptible to facilitated lattice oxygen depletion (Figure S3, Supporting Information) and transform above T = 670 K into complete rod-like structures (Figure 1d). Related changes are induced by water elimination and occur in conjunction with the phase transformation of the solid (Figures 1d and 3e,f). The resulting TiO_2 nanorods adopt the anatase structure and display high aspect ratios.[35,62,63] A mechanism that rationalizes the respective annealing-induced transformation has been proposed by Morgado et al.[64] Progressing dehydration initiates the shrinkage of the average interlayer distance between the titanate nanosheets and induces a topotactic structural condensation process,[64] in the course of which the [TiO_6] octahedra that constitute the titanate nanosheets shift to positions consistent with those of the anatase phase. Apart from the high aspect ratio, vacuum-annealed anatase nanorods show relatively smooth surfaces (Figure 1d, right image). These observations are reminiscent of studies[23,58] where the preferential elongation of anatase structures in the anatase [001] direction was reported for samples that were derived from hydrothermal treatment and subjected to acidic conditions thereafter. The zigzag configuration of the edge-sharing [TiO_6] octahedra comprising the nanotube walls structurally resembles the (100) planes of the TiO_2 anatase modification.[25,26] In summary, the annealing-induced tube-to-rod transformation that starts with scrolled up $H_2Ti_3O_7$ sheets and ends with the emergence of TiO_2 anatase nanorods is driven by dehydration and proceeds via the stepwise contraction of the interlayer distance between the titanate nanosheets. On the other hand, morphology and structure of $Na_2Ti_3O_7$ nanowires survive vacuum annealing up to temperatures of T = 870 K.

Excitonic Properties of the Nanostructures' Bulk. The photoelectronic properties of $Na_2Ti_3O_7$ nanowires and $H_2Ti_3O_7$ nanotubes clearly underline how the solids' morphology affects the nature and dynamics of the electronic excitation. With respect to the absorption threshold, the UV diffuse reflectance spectra of TiO_2 anatase particles as well as those of the titanate nanostructures are identical,[30] an observation which is in line with theoretical predictions.[65] With regard to photoluminescence, the respective properties of $Na_2Ti_3O_7$ nanowires are character-

(52) Li, G. H.; Ciston, S.; Saponjic, Z. V.; Chen, L.; Dimitrijevic, N. M.; Rajh, T.; Gray, K. A. *J. Catal.* **2008**, *253*, 105–110.
(53) Dimitrijevic, N. M.; Saponjic, Z. V.; Rabatic, B. M.; Poluektov, O. G.; Rajh, T. *J. Phys. Chem. C* **2007**, *111*, 14597–14601.
(54) Scotti, R.; Bellobono, I. R.; Canevali, C.; Cannas, C.; Catti, M.; D'Arienzo, M.; Musinu, A.; Polizzi, S.; Sommariva, M.; Testino, A.; Morazzoni, F. *Chem. Mater.* **2008**, *20*, 4051–4061.
(55) Stankic, S.; Müller, M.; Diwald, O.; Sterrer, M.; Knözinger, E.; Bernardi, J. *Angew. Chem., Int. Ed.* **2005**, *44*, 4917–4920.
(56) Müller, M.; Sternig, A.; Stankic, S.; Stöger-Pollach, M.; Bernardi, J.; Knözinger, E.; Diwald, O. *J. Phys. Chem. C* **2008**, *112*, 9120–9123.
(57) Li, G.; Dimitrijevic, N. M.; Chen, L.; Nichols, J. M.; Rajh, T.; Gray, K. A. *J. Am. Chem. Soc.* **2008**, *130*, 5402–5403.
(58) Wen, P.; Itoh, H.; Tang, W.; Feng, Q. *Langmuir* **2007**, *23*, 11782–11790.
(59) Mogilevsky, G.; Chen, Q.; Kulkarni, L. H.; Kleinhammes, A.; Mullins, W. M.; Wu, Y. *J. Phys. Chem. C* **2008**, *112*, 3239–3246.
(60) Mogilevsky, G.; Chen, Q.; Kleinhammes, A.; Wu, Y. *Chem. Phys. Lett.* **2008**, *480*, 517–520.
(61) One part of the controversy concerning the structural properties of this interesting class of material is related to the fact that adsorption of water and other species as well as the nature of the interface in general (solid−gas versus solid−liquid) determine structure and morphology. Changing the solvent or sample transfer into the vacuum chamber of a transmission electron microscope may critically affect these properties, and corresponding procedures require careful documentation.
(62) Tsai, C. C.; Teng, H. *Chem. Mater.* **2004**, *16*, 4352–4358.
(63) Thorne, A.; Kruth, A.; Tunstall, D.; Irvine, J. T. S.; Zhou, W. Z. *J. Phys. Chem. B* **2005**, *109*, 5439–5444.
(64) Morgado, E., Jr.; Jardim, P. M.; Marinkovic, B. A.; Rizzo, F. C.; de Abreu, M. A. S.; Zotin, J. L.; Arújo, A. S. *Nanotechnology* **2007**, *18*, 495710.

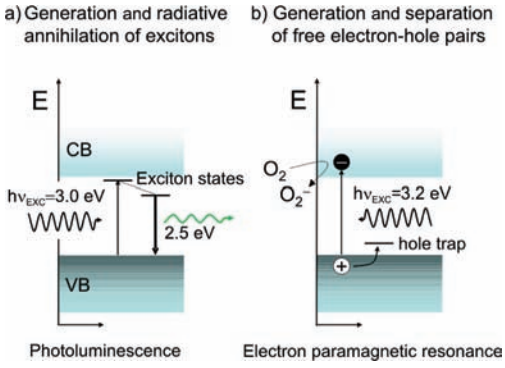

Figure 9. Simplified energy level diagrams that illustrate the UV light-induced processes of radiative exciton annihilation (a) that take action in $Na_2Ti_3O_7$ nanowires, on the one hand, and the formation of electron−hole pairs (b) that become dissociated by local fields in scrolled up $H_2Ti_3O_7$ nanotubes upon free charge carrier generation, on the other.

ized by an emission band at $h\nu = 2.5 \pm 0.1$ eV (Figure 5a), which was also observed on related $K_2Ti_3O_7$ structures as well as on the anatase particles.[30] We attribute this effect to trapped excitons within the $[TiO_6]$ units.[66−70] The PL excitation spectrum in Figure 5b shows that a photon energy of 3.0 eV is sufficient for the generation of excitons, the energy of which is smaller than the optical bandgap by the free exciton binding energy of 0.2 eV (Figure 5b). As schematized in Figure 9a, after photoexcitation, the subsequent step of exciton trapping is associated with an energy decrease by 0.5 eV. Finally, the radiative annihilation step produces photoluminescence emission light, which peaks at $h\nu = 2.5 \pm 0.1$ eV.

We checked for surface-related effects on photoluminescence emission and changed the sample atmosphere from high vacuum at pressures $p < 10^{-5}$ mbar to gaseous oxygen (10 mbar), a procedure that, in case of surface photoluminescence effects, leads to quenching:[71] irrespective of the high surface-to-volume-ratios of the materials investigated, no intensity changes were observed. Consequently, exciton formation and its radiative annihilation do not respond to changes at the surface of the respective nanostructure and must be ascribed to the bulk of the material. As a feature of excitons, the spatial extent of the excited state is determined by electronic coupling among the repeat units making up the material.[72] In the case of TiO_2-based structures, the excitonic properties depend on the $[TiO_6]$ octahedron's coordination state within the crystal structure, and there is general agreement about the fact that the formation of trapped excitons is favored in structures with lower coordination numbers of the repeat units. Such a situation applies more for $Na_2Ti_3O_7$ nanowires as compared to TiO_2 anatase (Figure 9).[73,74]

We observed a substantial depletion of PL emission on $Na_2Ti_3O_7$ samples that were activated at higher temperatures prior to PL measurements and believe that the annealing procedures, carried out under vacuum conditions and subsequently in oxygen atmosphere, are associated with a loss in periodicity of the $[TiO_6]$ subunits, which enhances the nonradiative deactivation pathway. In fact, Raman spectra related to annealed $Na_2Ti_3O_7$ nanowires (Figure 3) evidence that a small fraction of the material has been transformed into anatase, indicating a reduction and thus a substantial modification of the interlayer region, which expectedly becomes depleted of Na^+ ions.

On the other hand, the position and binding state of the protons within the interlayer region of scrolled-up $H_2Ti_3O_7$ nanotubes are different from those of the alkali ions.[75] The distortion of the protonated octahedron[30] is expected to suppress the path of trapped exciton formation and annihilation (Figure 5). Therefore, photons with energies equal to or larger than the optical bandgap $h\nu > 3.2$ eV produce free charge carriers (Figure 9b) instead of excitons (Figure 9a). Charge separation is additionally favored because titanate nanotubes represent curved structures where elastic strain gradients can generate electric polarization of the lattice.[76] Related fields exert a force on the electron and the hole separately and facilitate charge separation and interfacial electron transfer to surface adsorbed O_2. Molecular oxygen, in turn, promotes the efficiency of charge separation in comparison to the corresponding situation under vacuum by a factor of 2, an observation that emphasizes the important role of the interface in the overall photochemical reaction.[49] On $H_2Ti_3O_7$ nanotubes and the anatase nanorods derived therefrom (Figure 8), we observed two major trends: first, on hydroxylated nanotubes, trapped hole centers escape EPR detection (Figure 7a and f). This is attributed to constitutional OH groups present at the interfaces of the curved titanate nanosheets. We expect that these hydroxyls mediate the transformation of trapped holes into diamagnetic products via short-lived $OH^{\cdot}$ radicals as intermediates.[77,78] Second, surface adsorbed O_2^- ions that can be probed with EPR spectroscopy after photoexcitation can be efficiently stabilized at OH covered oxide surfaces (Figure 4).[79] As a consequence of annealing at elevated temperatures, surface hydroxyls become depleted (Figure 4), and the surface areas of the respective nanostructures become reduced as well. In terms of the spectroscopic fingerprints of trapped charge carriers, we found that the abundance of adsorbed O_2^- ions is relatively diminished as compared to that of trapped holes (O^- radicals), which increases. After annealing of the material to $T = 870$ K, the transformation of $H_2Ti_3O_7$ nanotubes into TiO_2 anatase nanorods is completed (Figures 1d and 3f). On these structures, the concentration of scavenged electrons turns out to be below that of O^- radicals, representing the positively charged counterparts. In addition, the overall yield of separated charges corresponds to only a quarter of that measured for TiO_2 anatase nanocrystals grown by metal organic chemical vapor deposition (Figure 8).[49] To rationalize this diminished yield of separated charges, one has to take into account that $H_2Ti_3O_7$ nanotubes contain a residual amount of Na^+ ions (~3 at. %) that remains after surface

(65) Enyashin, A. N.; Seifert, G. *Phys. Status Solidi B* **2005**, *242*, 1361–1370.
(66) Amtout, A.; Leonelli, R. *Solid State Commun.* **1992**, *84*, 349–352.
(67) (a) Sekiya, T.; Tasaki, M.; Wakabayashi, K.; Kurita, S. *J. Lumin.* **2004**, *108*, 69–73. (b) Wakabayashi, K.; Yamaguchi, Y.; Sekiya, T.; Kurita, S. *J. Lumin.* **2005**, *112*, 50–53.
(68) De Haart, L. G. J.; De Vries, A. J.; Blasse, G. *J. Solid State Chem.* **1985**, *59*, 291–300.
(69) Toyozawa, Y. *J. Lumin.* **1976**, *12/13*, 13–21.
(70) Song, K. S.; Williams, R. T. *Self-trapped Excitons*, 2nd ed.; Springer: Berlin, 1996; Vol. 105.
(71) Stankic, S.; Sterrer, M.; Hofmann, P.; Bernardi, J.; Diwald, O.; Knözinger, E. *Nano Lett.* **2005**, *5*, 1889–1893.
(72) Scholes, G. D.; Rumbles, G. *Nat. Mater.* **2006**, *5*, 683–696.
(73) Tang, H.; Lévy, F.; Berger, H. P.; Schmid, E. *Phys. Rev. B* **1995**, *52*, 7771–7774.
(74) In rutile, as the TiO_2 modification with the highest density, the coordination number of the TiO_6 octahedron corresponds to $Z = 10$ and is higher than in anatase, $Z = 8$, or in the related titanates, $Z \leq 8$.
(75) Zhang, S.; Chen, Q.; Peng, L.-M. *Phys. Rev. B* **2005**, *71*, 014104.
(76) Gross, L. E. *J. Mater. Sci.* **2006**, *41*, 53–63.
(77) Micic, O. I.; Zhang, Y. N.; Cromack, K. R.; Trifunac, A. D.; Thurnauer, M. C. *J. Phys. Chem. B* **1993**, *97*, 7277–7283.
(78) Murakami, Y.; Endo, K.; Ohta, I.; Nosaka, A. Y.; Nosaka, Y. *J. Phys. Chem. C* **2007**, *111*, 11339–11346.
(79) Diwald, O.; Knözinger, E. *J. Phys. Chem. B* **2002**, *106*, 3495–3502.

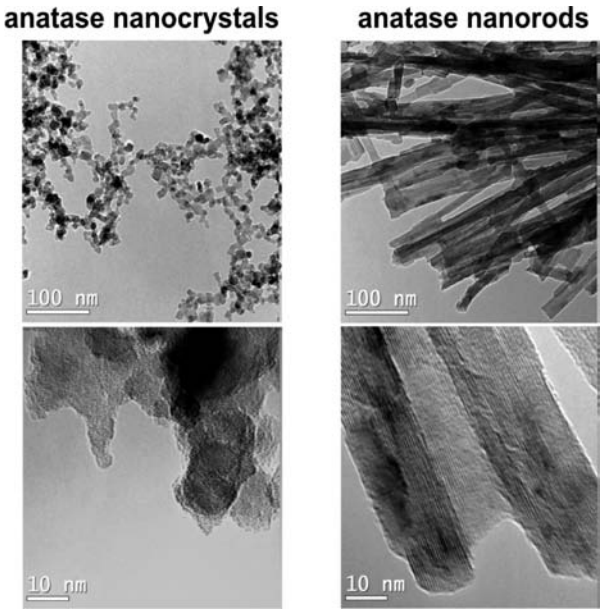

Figure 10. Transmission electron micrographs of anatase nanocrystals grown by metal organic chemical vapor deposition (left panel) and anatase nanorods derived from vacuum-annealed titanate nanotubes (right panel).

Table 2. Fundamental Particle Properties, Particle Ensemble Characteristics, and Charge Separation Yields Related to Anatase Nanocrystals and Anatase Nanorods Described by Figure 9[a]

	anatase nanocrystals	anatase nanorods
$S_{BET}/m^2\ g^{-1}$	130 ± 10	77 ± 10
$d_{particle}/nm$	13 ± 2	16 ± 5
$L_{particle}/nm$	13 ± 2	100 ± 40
aspect ratio	1 ± 0	6 ± 3
$O^-/\mu mol\ g^{-1}$	4 ± 2	1 ± 1
$O_2^-/\mu mol\ g^{-1}$	4 ± 2	0.4 ± 0
$O^-/nmol\ m^{-2}$	31 ± 10	15 ± 7
$O_2^-/nmol\ m^{-2}$	31 ± 10	5 ± 2

[a] The respective numbers are juxtaposed for the sake of comparison.

chemistry-induced transformation of $Na_2Ti_3O_7$ nanowires into $H_2Ti_3O_7$ nanotubes.[29] Such remnants still act as impurities that facilitate the radiative deactivation of photoexcited states and thus substantially decrease the yield of separated charges (Figure 8).

Figure 10 compares electron microscopy data between airborne anatase nanocrystals obtained by metal organic chemical vapor deposition (MOCVD) and morphologically better defined anatase nanorods derived from vacuum-annealed $H_2Ti_3O_7$ nanotubes. Fundamental particle properties of the surface dehydroxylated powders are specified in Table 2. Despite comparable dispersion and lateral particle extension, the associated surface structures are very different on the nanoscale. The irregular morphology of MOCVD grown particles is clearly demonstrated by the high-resolution electron microscopy image in the left panel of Figure 10. They lack any type of surface faceting, which points to high structural disorder at the interface.[80] However, TiO_2 anatase nanorods exhibit a high concentration of flat surface regions, which presumably correspond to anatase (100) faces.[25,26] On these structures, the measured amount of trapped hole centers O^- ions does not have a corresponding concentration of their electronic counterpart, that is, scavenged electrons. The absence of the latter species must be attributed to the strongly reduced number of low coordinated surface Ti cations that qualify for O_2^- stabilization.[46,47] The enhanced charge separation reached by UV exposure in the presence of gaseous O_2 in combination with different O_2^- yields determined on TiO_2 nanostructures with different levels of surface defectivity clearly underlines the critical role of the interface the respective nanostructure shares with the gasphase. In summary, whereas the deactivation of photoexcited states in $Na_2Ti_3O_7$ nanowires is subject to the bulk, charge separation as well as the fate of photogenerated charge carriers are determined by the interface properties of the respective nanostructure. Finally, it is interesting to look at the concentrations of separated charges as plotted in Table 2 in the context of materials quantities used. Typical sample masses for various types of spectroscopy experiments correspond to approximately 20 mg. Considering that the MOCVD anatase particles used exhibit a particularly narrow size distribution with an average particle size of 13 nm and the fact that hole centers are exclusively trapped at the particle surface,[41,49] we conclude that only a fraction of 10^{-4} surface atoms is involved in persistent charge trapping as evidenced in the present study. Similar experiments with micrometer-sized particles having surface areas below 1 $m^2\ g^{-1}$ would require several grams of sample. The fact that such quantities cannot be reliably sampled with molecular spectroscopy techniques anymore points to the importance of nanomaterials with associated high surface-to-volume ratios for the spectroscopic investigation of oxide particle surfaces.

Conclusions

We comprehensively explored the photolectronic properties of various forms of TiO_2-based nanostructures, that is, $H_2Ti_3O_7$ nanotubes and $Na_2Ti_3O_7$ nanowires obtained by solution-based synthesis as well as different types of TiO_2 anatase nanocrystals, and evaluated the relative contribution of composition and structure of bulk and surface on the branching between chemical utilization of photogenerated charges and the annihilation of photoexcited states. While photoluminescence was found to be entirely a bulk process, trapping and interfacial transfer of photogenerated charges clearly depends on the condition of the interface. Considering the complexity of the function "photocatalytic activity" with respect to the performance of nanoparticle powders, the presented quantitative assessment points to ways to differentiate between material specific determinants and thus provides a methodological benchmark for a more effective and comparable characterization of new materials' photoactivities.

Acknowledgment. This work was financially supported by the Austrian Fonds zur Förderung der Wissenschaftlichen Forschung (FWF − P17514-N11/P19702-N20), which is gratefully acknowledged. We thank Dr. Hinrich Grothe for his assistance with the Raman measurements and Dr. Andrea Vittadini for valuable discussions.

Supporting Information Available: Additional TEM data, electron paramagnetic resonance, UV−vis diffuse reflectance and photoluminescence spectra related to oxidized and vacuum-annealed titanate nanostructures, as well as FT-IR spectra of dehydroxylated $Na_2Ti_3O_7$ nanowires. This material is available free of charge via the Internet at http://pubs.acs.org/.

JA810109G

(80) For reasons of feasibility, it is beyond the scope of the present study to estimate the level of surface defectivity in terms of low coordinated surface sites and other types of point defects on the basis of HR-TEM data.